REPORT DOCUMENTATION PAGE

Form Approved OMB NO. 0704-0188

The public reporting burden for this collection of information is estimated to average 1 hour per response, including the time for reviewing instructions, searching existing data sources, gathering and maintaining the data needed, and completing and reviewing the collection of information. Send comments regarding this burden estimate or any other aspect of this collection of information, including suggesstions for reducing this burden, to Washington Headquarters Services, Directorate for Information Operations and Reports, 1215 Jefferson Davis Highway, Suite 1204, Arlington VA, 22202-4302. Respondents should be aware that notwithstanding any other provision of law, no person shall be subject to any oenalty for failing to comply with a collection of information if it does not display a currently valid OMB control number.
PLEASE DO NOT RETURN YOUR FORM TO THE ABOVE ADDRESS.

1. REPORT DATE (DD-MM-YYYY)	2. REPORT TYPE	3. DATES COVERED (From - To)
31-08-2015	Conference Proceeding	-

4. TITLE AND SUBTITLE
Shock Wave Propagation in Cementitious Materials at Micro/Meso Scales

5a. CONTRACT NUMBER
W911NF-11-2-0043

5b. GRANT NUMBER

5c. PROGRAM ELEMENT NUMBER
611104

6. AUTHORS
M. Nelms, A. M. Rajendran, W. Hodo, R. Mohan

5d. PROJECT NUMBER

5e. TASK NUMBER

5f. WORK UNIT NUMBER

7. PERFORMING ORGANIZATION NAMES AND ADDRESSES
North Carolina A&T State University
1601 East Market Street

Greensboro, NC 27411 -0001

8. PERFORMING ORGANIZATION REPORT NUMBER

9. SPONSORING/MONITORING AGENCY NAME(S) AND ADDRESS (ES)
U.S. Army Research Office
P.O. Box 12211
Research Triangle Park, NC 27709-2211

10. SPONSOR/MONITOR'S ACRONYM(S)
ARO

11. SPONSOR/MONITOR'S REPORT NUMBER(S)
59544-MA-PIR.25

12. DISTRIBUTION AVAILIBILITY STATEMENT
Approved for public release; distribution is unlimited.

13. SUPPLEMENTARY NOTES
The views, opinions and/or findings contained in this report are those of the author(s) and should not contrued as an official Department of the Army position, policy or decision, unless so designated by other documentation.

14. ABSTRACT
Shock wave response of heterogeneous materials like cement and concrete is greatly influenced by the constituents and their statistical distributions. The microstructure of cement is complex due to the presence of unhydrated water, nano/micro pores, and other hydrated and unhydrated products, such as the C-S-H gel, tri-calcium silicate, di-calcium silicate etc. The evolved microstructures at different degrees of hydration are captured using a suite of software that explicitly modeled the chemical compositions of various constituents and their byproducts for a water/cement ratio of 0.4. An evolved microstructure of 50x50x50 micron3 volume of Portland cement product was

15. SUBJECT TERMS
shock propagation, micro and macro scales, finite element modeling

16. SECURITY CLASSIFICATION OF:			17. LIMITATION OF ABSTRACT	15. NUMBER OF PAGES	19a. NAME OF RESPONSIBLE PERSON
a. REPORT	b. ABSTRACT	c. THIS PAGE			Ram Mohan
UU	UU	UU	UU		19b. TELEPHONE NUMBER 336-285-2867

Standard Form 298 (Rev 8/98)
Prescribed by ANSI Std. Z39.18

Report Title

Shock Wave Propagation in Cementitious Materials at Micro/Meso Scales

ABSTRACT

Shock wave response of heterogeneous materials like cement and concrete is greatly influenced by the constituents and their statistical distributions. The microstructure of cement is complex due to the presence of unhydrated water, nano/micro pores, and other hydrated and unhydrated products, such as the C-S-H gel, tri-calcium silicate, di-calcium silicate etc. The evolved microstructures at different degrees of hydration are captured using a suite of software that explicitly modeled the chemical compositions of various constituents and their byproducts for a water/cement ratio of 0.4. An evolved microstructure of 50x50x50 micron3 volume of Portland cement product was modeled as a representative volume element (RVE) through a general purpose finite element code, ABAQUS®. The heterogeneity induced shock decay phenomenon under compression in this 50-micron size cube due to an OFHC Copper flyer plate impact is analyzed.

Conference Name: 19th Biennniel Conference of the APS Topical Group on Shock Compression of Condensed Matter
Conference Date:

Shock Wave Propagation in Cementitious Materials at Micro/Meso Scales

M. Nelms[1], A.M. Rajendran[1,a)], W. Hodo[2], and R. Mohan[3]
[1]*Department of Mechanical Engineering, University of Mississippi, University, MS*
[2]*U.S. Army Engineer Research and Development Center, Vicksburg, MS*
[3]*Joint School of Nano science and Nano engineering, North Carolina A&T State University, Greensboro, NC*
[a)]*Corresponding author: raj@olemiss.edu*

Abstract. Shock wave response of heterogeneous materials like cement and concrete is greatly influenced by the constituents and their statistical distributions. The microstructure of cement is complex due to the presence of unhydrated water, nano/micro pores, and other hydrated and unhydrated products, such as the C-S-H gel, tri-calcium silicate, di-calcium silicate etc. The evolved microstructures at different degrees of hydration are captured using a suite of software that explicitly modeled the chemical compositions of various constituents and their byproducts for a water/cement ratio of 0.4. An evolved microstructure of 50x50x50 micron^3 volume of Portland cement product was modeled as a representative volume element (RVE) through a general purpose finite element code, ABAQUS®. The heterogeneity induced shock decay phenomenon under compression in this 50-micron size cube due to an OFHC Copper flyer plate impact is analyzed.

INTRODUCTION

During the past few decades, there have been sporadic efforts using plate impact experimental data to understand shock decay in cement and concrete. Various heterogeneities in these materials strongly influenced the dispersion and attenuation characteristics of shock waves. Several investigators [1-5] studied the shock wave response of concrete using so called hydrocodes as well as employing empirically based material strength models. Kipp, Chhabildas, and Reinhart [2] showed wave dispersion in concrete under elastic regimes by measuring the free surface velocity at different spatial locations on the stress free rear surface. The three dimensional CTH [6] simulations employing a continuum constitutive model used a 200 micron (0.2 mm) mesh resolution to explicitly model the aggregates. The heterogeneity was modeled by an ellipsoidal inclusion surrounded by the grout material in a cylinder. The CTH results also showed pulse dispersion and matched the measured wave profiles. The researchers in Cavendish laboratory [3-4] reported both dynamic strength and shock Hugoniot of cementitious materials through plate impact experimental studies. Buzaud et al [5] modeled shock compression under very high pressure due to projectile penetration or contact detonation. These authors also experimentally captured wave dispersion in concrete. There is hardly any reported modeling under shock loading conditions that explicitly describes each constituent, including the free water and microvoids in the cement with their individual elastic properties. Most finite element method based analyses of wave propagation in concrete utilized a continuum damage model with average effective properties. The attenuation was described using a RVE with ellipsoidal particles in an isotropic and homogeneous matrix [5]. These studies however did not explicitly describe pulse attenuation or the shock decay due to the presence of heterogeneities as it propagated from the impact surface towards the back surface of the target. For concrete materials, the average sizes of the aggregates influence the elastic properties and shock attenuation characteristics. Therefore, it is important to establish appropriate length scales in computational modeling as well as the sample size in experiments. To further understand the complex shock decay in concrete, the present computational study on wave propagation in cementitious materials is based on a Portland cement (Type I) without any sand and large aggregates (like stones). The absence of these materials enables modeling with one micron resolution at the mesoscales.

DESCRIPTION OF CEMENTITIOUS MATERIALS

Cement is a highly heterogeneous material comprised of several microscale constituents that bind through chemical reaction with the addition of water and uses its covalent bonding mechanisms. C-S-H has the highest volume fraction and is believed to be responsible for controlling the engineering properties. When limestone and clay are fused together at 1450^0C, clinker nodules are formed. Hydration kinetic reactions form the cement products and form the binder between the various clinkers. The clinker is typically comprised of tricalcium silicate (C_3S), dicalcium silicates (C_2S), tricalcium aluminates (C_3A), and gypsum. Typically, cementitious materials are combined with fine (sand) and course (aggregates) to create structural concrete mixtures. The constituents vary depending on the specific application, so for the current study a general Portland cement is used.

The tricalcium silicates are responsible for the strength development from 0 to 28 days. The dicalcium silicates are responsible for the strength development after 28 days. The C-S-H is the reaction product formed during hydration of cement and is the most important constituent that binds together all constituent material particles. For instance, nanostructures of C-S-H gel have been determined for Jennite or Tobermorite ores. Recently Murillo et al., [7] reported the elastic properties of the clinkers and the C-S-H (Tobermorite-14 Å) gel based on their molecular dynamics (MD) simulations and experimental data. The cementitious material modeled in this study contained 17 different microconstituents with varying properties and are presented in Table 1. The elastic moduli show significant variation, ranging from 22.4 to 117.6 GPa, thereby producing wave speed and impedance dissimilarities at the microscale.

TABLE 1. Elastic properties of the cement RVE microconstituents

Microconstituent	E (GPa)	ν
Calcium Silicate Hydrate Gel (CSH)	22.4	0.25
Calcium Hydroxide (CH)	42.3	0.324
Water Filled Porosity (H_20)	1	0.49924
Monsulfate AFM (C_4ASH_{12})	22.4	0.25
Hydrogarnet (C_3AH_6)	22.4	0.25
Tricalcium Silicate (C_3S)	117.6	0.314
Ettringite ($C_6AS_3H_{32}$)	22.4	0.25
Dicalcium Silicate (C_2S)	117.6	0.314
Iron-rich Stable Ettringite ($ETTRC_4AF$)	22.4	0.25
Empty Porosity	1	0
Tricalcium Aluminate (C_3A)	117.6	0.314
Tetracalcium Aluminoferrite (C_4AF)	117.6	0.314
Iron Hydroxide (FH_3)	22.4	0.25
Hemihydrite and Anhydrite (GYPSUMS)	45.7	0.33
Dihdyrate (Gypsum) (CSH_2)	45.7	0.33
ABSGYPS	45.7	0.33
Hemihydrate ($CSH_{1/2}$)	62.9	0.3

Table 2 provides the wave speed, impedance and interaction between microconstituents. R is the reflected shock wave energy, σ_r is the reflected stress and σ_t is the transmitted stress between an empty or water filled pore and the RVE microconstituents when subjected to a unit shock stress. Of particular interest is the interaction between empty and water filled pores with the various cementitious materials. The empty pores, as expected, behave like internal free surfaces and the water shows a similar response. The reflected stress ratios range from -0.62 to -0.89. The presence of these two types of porosity are a dominant factor for dispersive nature of Portland cement. The empty pores are a result of chemical shrinkage that occurs during the cement hydration process. In addition, the statistically random spatial distribution of the 17 microconstituents create internal impedance mismatches that also influence the heterogeneous materials' wave dispersion characteristics thus requiring explicit computational modeling of the cementitious microstructure.

TABLE 2. Properties of individual constituents

Microconstituent	Vol. Frac. (%)	Wave speed (μm/ns)	Density (kg/m^3)	Impedance (MPa*s/m)	R (H_2O)	R (pore)	σ_t (H_2O)	σ_r (H_2O)	σ_t (pore)	σ_r (pore)
Calcium Silicate Hydrate Gel (CSH)	42.35	3.809	2240	8.53	0.45	0.59	0.33	-0.67	0.01	-0.99
Calcium Hydroxide (CH)	16.26	5.566	2733	15.21	0.60	0.71	0.22	-0.78	0.00	-1.00
Water Filled Porosity (H_20)	15.21	1.481	1000	1.48	0.00	0.04	1.00	0.00	0.04	-0.96
Monsulfate AFM (C_4ASH_{12})	5.97	0.174	2015	0.35	0.44	0.58	0.34	-0.66	0.17	-0.83
Hydrogarnet (C_3AH_6)	4.47	3.266	2520	8.23	0.48	0.61	0.31	-0.69	0.01	-0.99
Tricalcium Silicate (C_3S)	4.35	7.170	3210	23.02	0.77	0.84	0.12	-0.88	0.00	-1.00
Ettringite ($C_6AS_3H_{32}$)	3.35	3.976	1700	6.76	0.41	0.55	0.36	-0.64	0.01	-0.99
Dicalcium Silicate (C_2S)	2.36	8.508	2280	19.40	0.77	0.84	0.12	-0.88	0.00	-1.00
Iron-rich Ettringite ($ETTRC_4AF$)	1.70	3.864	1800	6.96	0.42	0.56	0.35	-0.65	0.01	-0.99
Empty Porosity	1.28	0.032	1000	0.03	0.04	0.00	1.00	0.00	1.00	0.00
Tricalcium Aluminate (C_3A)	1.08	7.380	3030	22.36	0.77	0.84	0.12	-0.88	0.00	-1.00
Tetracalcium Aluminoferrite (C_4AF)	0.87	7.170	3210	23.02	0.79	0.85	0.11	-0.89	0.00	-1.00
Iron Hydroxide (FH_3)	0.43	2.993	3000	8.98	0.51	0.64	0.28	-0.72	0.01	-0.99
Hemihydrite and Anhydrite	0.32	5.413	2311	12.51	0.62	0.73	0.21	-0.79	0.01	-0.99
Dihdyrate (Gypsum) (CSH_2)	0.0009	6.652	3730	24.81	0.62	0.73	0.21	-0.79	0.00	-1.00
ABSGYPS	0.0003	5.413	2311	12.51	0.62	0.73	0.21	-0.79	0.01	-0.99
Hemihydrate ($CSH_{1/2}$)	0.0001	5.402	2320	12.53	0.65	0.75	0.19	-0.81	0.01	-0.99
Average	100	3.784	2153	9.03	0.50	0.63	0.29	-0.71	0.01	-0.99
Copper *(Flyer)*	100	4.635	8940	41.44	0.87	0.91	0.07	-0.93	0.00	-1.00

COMPUTATIONAL MODELS

The micro-structure voxel information from NIST software CEMHYD3D [8] for a given particle distribution is imported into the general purpose ABAQUS® finite element code using an in-house developed Matlab® code and modeled as a micro-scale representative volume element (RVE) using continuum hexahedral elements to generate RVEs 50x50x50 microns in dimension (125K). Figure 2a is the resulting RVE microstructure, Fig. 2b is the water filled porosity and Fig. 2c is the empty porosity distribution. A plate impact configuration was simulated to fundamentally understand the shock wave decay phenomenon.

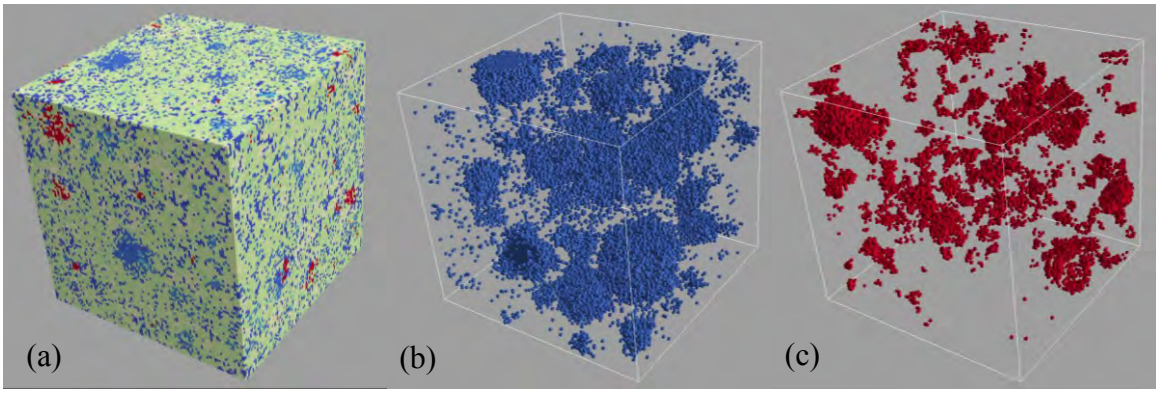

FIGURE 1. (a) CEMHYD3D generated cementitious RVE including the explicitly modeled (b) water and (c) empty porosity

The microstructures for a given particle distribution of various constituents are explicitly modeled in ABAQUS® as a 50 micron cube RVE. Shahzamanian et al. [10], determined the effective elastic tensor by applying kinematic and

periodic boundary conditions to the RVE and by using individual Young's Modulus and Poisson's ratio for each of the constituents described in Table 2. The effective Young's Modulus was 24 GPa and Poisson's ratio was 0.33 for the RVE. The average wave speed was 3.784 μm/ns (see Table 2). Similar values have been found in open literature [11].

In the computer simulation, an 11 μm thick copper flyer plate was made to impact a 50 μm thick cement cube under one dimensional strain boundary condition at an arbitrary impact velocity of 570 m/s. Though the water channels are on the order of nanometers, in the present analysis one micron size was used to avoid humongous computing time. Roller boundary conditions were employed on the lateral surfaces to mimic macroscale 1-D strain while the rear surfaces were kept as stress free. The RVE was subject to flyer plate impact under one-dimensional strain boundary condition. Internally, the elements were allowed to deform in all directions to capture the 3-D interaction of microconstituents.

RESULTS AND DISCUSSIONS

To understand wave decay due to the presence of heterogeneity, modeling and simulations were performed for two cases: a) pure elastic response, and b) elastic-plastic with tensile damage. Under compression the microconstituents are modeled using perfectly plastic material behavior. The tensile damage was implemented using the model developed by Taylor, Chen and Kuszmaul and validated for brittle rocks [12] and ceramics [13].

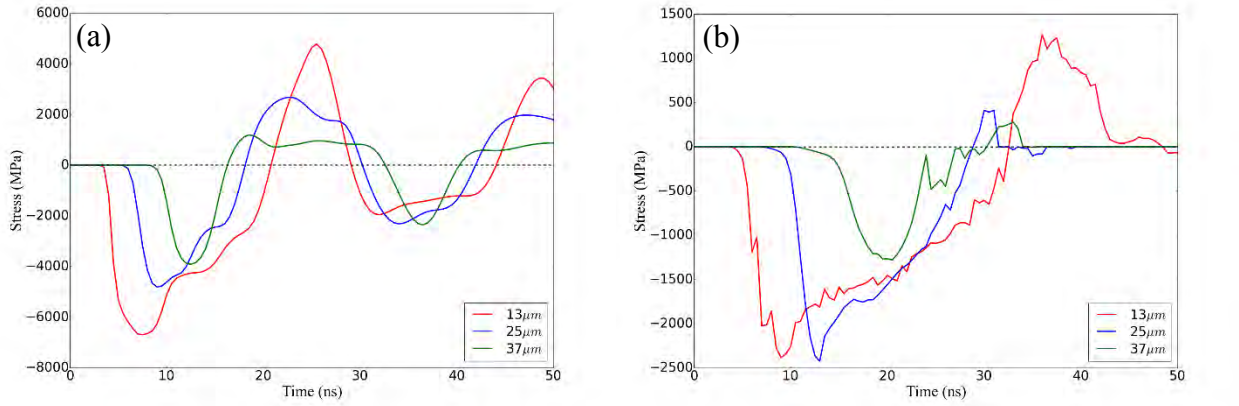

FIGURE 2. (a) Elastic behavior with no tensile damage and (b) elastic – plastic behavior with tensile damage.

Figure 2a describes wave attenuation (decreasing stress amplitude as the wave propagates into the cement target) due to impedance mismatch between the various constituents. The maximum stress in compression is much larger than the stress in tension. The release wave from the rear surface of the flyer plate releases stress in compression. The attenuation is significant in both compression and tension. In this simulation, a 50 μm thick target was used. Therefore, these distances are 1/4th, 1/2, and 3/4th from the impact plane. While the pulse duration at 13 μm distance from the impact plane remains under compression for about 15 to 17 nanoseconds, the release wave from the stress-free back surface of cement plate decreases the pulse durations in compression at locations (25 μm and 37 μm) closer to the rear surface of cement.

In Fig. 2b, the wave attenuation behaviors for the case where the cement experiences both inelastic compression and tensile damage are shown. At 13 μm from the impact plane, the cement remains in compression for a long time until the release wave from the target rear surface arrives and goes into tension. In addition to decreasing stresses as the shock wave progresses through the RVE, the loading rate of the shock stress decreases and is more pronounced when accounting for the temporal plasticity and tensile damage. The damage seems to be incipient and therefore, the stress amplitude under tension is significantly higher (about 1250 MPa – shown in red) compared to the stress histories at 25 μm and 37 μm which are farther away from the impact surface. Table 3 is the wave arrival times at 1/4th, 1/2, 3/4th and rear surface distances from the impact plane. The release wave from the flyer arrives at 13 micron at 8.18 ns, 25 micron at 11.35 ns and 37 micron at 14.52 ns. The release waves converge at 41.05 micron at 15.58 ns.

TABLE 3. Wave arrival at various distance within the RVE

Distance (μm)	Compression Wave Arrival (ns)	Wave Speed (μm/ns)	Release Wave Arrival (ns)
13	3.44	3.779	8.18
25	6.61	3.782	11.35
37	9.78	3.814	14.52
50	13.01	3.785	19.26

As the tensile waves from the back surface of the OFHC copper and the cement target interact at these locations, the damage model softens the stress levels (less than about 500 MPa – green and blue). It can be seen from the green plot that the tensile stress is very low (250 MPa) and later becomes zero due to complete tensile damage (D=1); this location is nearest to the rear surface of the cement target compared to the other two locations. As the damage is partial at 25 μm, the tensile stress reaches a level of about 400 MPa. The pulse duration decreases with increasing distance from the impact plane indicating significant wave dispersion. The local wave reflections, due to impedance mismatching between various constituents, cause this dispersion as well as attenuation. The effective wave speed in the RVE, based on the average properties, was about 3.7 mm/μs (or micron/nanosecond). In these plots, the wave arrival times at these three locations was approximately about 3.6 to 3.7 mm matching the effective speed.

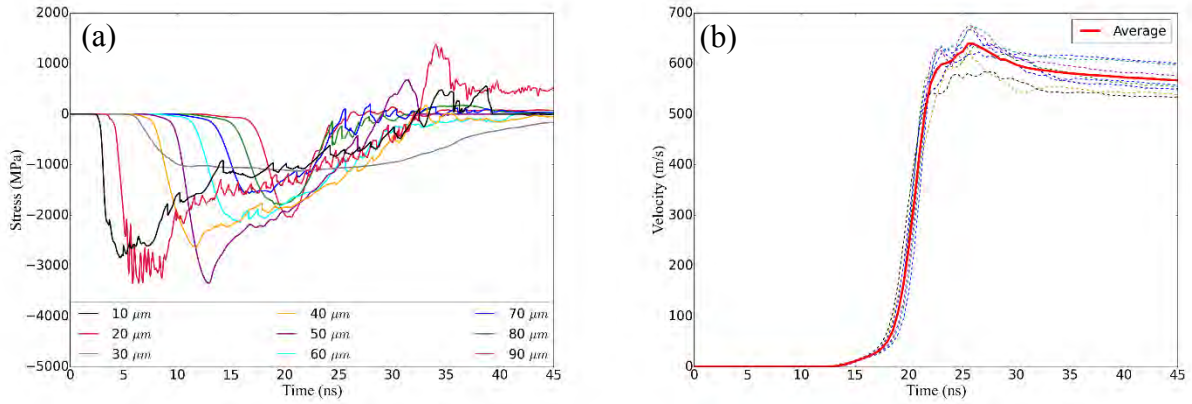

FIGURE 3. (a) Shock wave dispersion and attenuation and (b) velocity history at target's back surface

The wave attenuation is shown in Fig. 3a for nine different locations inside the cement target plate for Case 2 (elastic-plastic-tensile damage). The water containing elements seem to remain under compression for a longer duration compared to the solid elements. These plots clearly show that the wave histories at each location are different by exhibiting various degrees of wave attenuation and dispersion. The continuum models fail to show these complex wave decay phenomena due to the assumption of homogeneous and isotropic behaviors for a highly heterogeneous solid. Fig. 3b shows the free surface velocity at the back of the cement target. The velocity history is influenced by the properties of the constituent located at the numerically measured location. The average velocity for several elements in the back surface is also shown in Fig. 3b. Though the stress histories showed very strong attenuation and dispersion, the consolidated velocity profile resembles the VISAR measurement in a typical plate impact experiment with concrete targets [2].

SUMMARY

By explicitly modeling the individual constituents with their own elastic properties through a representative volume element, it is possible to capture the wave decay characteristics in finite element simulations. The release waves from the rear surfaces of both the flyer and cement target reduce pulse durations in regions closer to the target rear surface. The RVE results showed a strong wave dispersion and attenuation due to the complex wave reflections at the boundaries of various constituents in cement. The average response of the heterogeneous RVE, due to shock wave propagation, resembled the plate impact experimental velocity profile for an arbitrary concrete material. The average response was effectively an isotropic and homogeneous "equivalent" solid (or RVE) with some effective properties. Since the constituents are randomly distributed in cementitious materials, the response tends to follow

isotropic behaviors. The RVE approach provides a realistic methodology to estimate effective shock response of a heterogeneous solid, as well as highlight the necessity for explicitly modeling the microconstituents to determine macroscale material behavior during shock loading. Using the effective properties and by alleviating very expensive direct computer simulations in design applications, it may then be possible to perform shock response of a heterogeneous solid through continuum models.

ACKNOWLEDGMENTS

The authors from University of Mississippi, Oxford, and North Carolina A&T State University, Greensboro acknowledge the support by the U.S. Army Research Office under a cooperative agreement award contract No. W911NF-11-2-0043 (Program Manager: Dr. Joseph Myers) and the U.S. Army Engineering Research and Development Center's Military Engineering Basic/Applied "MMFP" Research Program. Additionally, discussions with several researchers at Engineering Research and Development Center, Vicksburg, MS, and U. S. Army Research Laboratory are gratefully acknowledged. The simulations were performed using at the US Army ERDC DoD Supercomputing Resource Center at Vicksburg, MS. The visualizations were developed with the aid of US Army ERDC Data Analysis and Assessment Center in Vicksburg, MS. Some of the calculations reported in this work were carried out on equipment at the Mississippi Center for Supercomputing Research (MCSR) funded by the National Science Foundation (CHE-1338056). The authors are grateful for the assistance provided by Dr. Brian Hopkins at MCSR.

REFERENCES

1. T. Antoun, "Constitutive/Failure Model for the Static and Dynamic Behaviors of Concrete Incorporating Effects of Damage and Anisotropy," a PhD Dissertation, University of Dayton, Dayton, Ohio, December 1991.
2. Kipp, M.E., Chhabildas. L.C., and Reinhart, W.D., "Elastic Shock Response and Spall Strength of Concrete," in Shock Compression in Condensed matter – 1997, edited by S.C., Schmidt et. Al., 1998 American Institute of Physics (AIP) Conference Proceedings 429, New York, 1998, pp. 557-560.
3. Tsembelis, K., Millett, J.C.F., Proud, W.G., and Field, J.E., "The Shock Hugoniot Properties of Cement Paste up to 5 GPa," in Shock Compression in Condensed matter – 1999, edited by M.D. Furnish, L.C. Chhabildas, and R.S. Hixson, 2000 American Institute of Physics (AIP) Conference Proceedings 429, New York, 1999, pp. 1267-1270.
4. Tsembelis, K., Proud, W.G., and Field, J.E., "The Dynamic Strength of Cement Paste Under Shock Compression," in Shock Compression in Condensed matter – 2001, edited by M.D. Furnish, N.N. Thadhani, and Y. Horie, 2002 American Institute of Physics (AIP) Conference Proceedings 429, New York, 2001, pp. 1414-1417.
5. E. Buzaud, P.L. Hereil, C. Pontiroli, and P. Lambert, "Modeling the Shock Compression of Concrete Under 20 GPa," in Shock Compression in Condensed matter – 2005, edited by M.D. Furnish, et al., 2005 American Institute of Physics (AIP) Conference Proceedings 0-7354-0341-4, NY, 2005, pp. 303-306.
6. McGlaun, J. Michael, S. L. Thompson, and M. G. Elrick. "CTH: a three-dimensional shock wave physics code." International Journal of Impact Engineering 10.1 (1990): 351-360.
7. John S Rivas Murillo, Ahmed Mohamed,Wayne Hodo, Ram V Mohan, A Rajendran and R Valisetty, "Computational modeling of shear deformation and failure of nanoscale hydrated calcium silicate hydrate in cement paste: Calcium silicate hydrate Jennite," International Journal of Damage Mechanics, pp. 1–17, 2015.
8. Bentz, D.P., 1997, "Three-Dimensional Computer Simulation of Portland Cement Hydration and Microstructure Development," J. Am. Ceram. Soc., 80(1), pp. 3-21.
9. ABAQUS (2015) Reference Manuals. Dassault Systèmes Simulia Corp., Providence, RI, USA
10. M.M.Shahzamanian, T.Tadepalli, A. M. Rajendran, W.D. Hodo, R. Mohan, R. Valisetty, P. W. Chung and J. J. Ramsey, "Representative Volume Element Based Modeling of Cementitious Materials" Journal of Engineering Materials and Technology, Vol 136, 2014.
11. Web reference: ciks.cbt.nist.gov/~garbocz/paper148/node3.htm
12. Taylor, Lee M., Er-Ping Chen, and Joel S. Kuszmaul. "Microcrack-induced damage accumulation in brittle rock under dynamic loading." Computer methods in applied mechanics and engineering 55.3 (1986): 301-320.
13. Rajendran, A. M., and J. L. Kroupa. "Impact damage model for ceramic materials." Journal of Applied Physics 66.8 (1989): 3560-3565.